AIP | APL Materials

Mesoporous tertiary oxides via a novel amphiphilic approach

Natasha Bennett, Annela M. Seddon, James E. Hallett, Winfried Kockelmann, Valeska P. Ting, Sajanikumari Sadasivan, Robert P. Tooze, and Simon R. Hall

Citation: APL Mater. **4**, 015701 (2016); doi: 10.1063/1.4930808
View online: http://dx.doi.org/10.1063/1.4930808
View Table of Contents: http://scitation.aip.org/content/aip/journal/aplmater/4/1?ver=pdfcov
Published by the AIP Publishing

Mesoporous tertiary oxides via a novel amphiphilic approach

Natasha Bennett,[1] Annela M. Seddon,[2,a] James E. Hallett,[2] Winfried Kockelmann,[3] Valeska P. Ting,[4] Sajanikumari Sadasivan,[5] Robert P. Tooze,[5] and Simon R. Hall[1,a]

[1]*Bristol Centre for Functional Nanomaterials, Centre for Nanoscience and Quantum Information, Tyndall Avenue, Bristol BS8 1FD, United Kingdom and Complex Functional Materials Group, School of Chemistry, University of Bristol, Bristol BS8 1TS, United Kingdom*

[2]*H.H. Wills Physics Laboratory, University of Bristol, Tyndall Avenue, Bristol BS8 1TL, United Kingdom*

[3]*STFC Rutherford Appleton Laboratory, Chilton OX11 0QX, United Kingdom*

[4]*Department of Chemical Engineering, University of Bath, Bath BA2 7AY, United Kingdom*

[5]*Sasol Technology (UK) Ltd, Purdie Building, North Haugh, St Andrews, Fife KY16 9ST, United Kingdom*

(Received 27 May 2015; accepted 31 August 2015; published online 28 September 2015)

We report a facile biomimetic sol-gel synthesis using the sponge phase formed by the lipid monoolein as a structure-directing template, resulting in high phase purity, mesoporous dysprosium- and gadolinium titanates. The stability of monoolein in a 1,4-butanediol and water mixture complements the use of a simple sol-gel metal oxide synthesis route. By judicious control of the lipid/solvent concentration, the sponge phase of monoolein can be directly realised in the pyrochlore material, leading to a porous metal oxide network with an average pore diameter of 10 nm. [http://dx.doi.org/10.1063/1.4930808]

Various approaches to oxide synthesis have been developed, ranging from traditional solid state syntheses[1–3] and vapour deposition[4–6] to sol-gel routes,[7,8] in order to produce high purity products with control over crystallite morphology. The synthesis of mesoporous oxides can be broadly classed as following one of two methodologies: hard templating, using materials such as silica to template metal oxide systems[9,10] and biomimetic soft templating with the use of surfactant templates, favoured for the ease of template removal via thermal decomposition.[11] In the case of the latter, there has been little use of type II amphiphiles (critical packing parameter $\gamma > 1$, forming inverse micelle structures) for templating in any inorganic system. The few studies that exist involve the synthesis of platinum with a single diamond bicontinuous cubic morphology,[12] mesoporous alumina,[13] and metal nanoparticles and nanorods.[14] Use of a type II amphiphile to produce tertiary metal oxides, however, is yet to be reported.

Lanthanide titanates ($Ln_2Ti_2O_7$ Ln = Dy, Gd) are tertiary metal oxides with the pyrochlore structure ($Fd3m$), which have recently received attention as spin frustrated systems and as neutron absorbers.[15–18] They are particularly suitable for nuclear applications as they have high melting points of ~1870 °C and 1820 °C for $Dy_2Ti_2O_7$ (DTO) and $Gd_2Ti_2O_7$ (GTO), respectively, high neutron absorption efficiency, modest swelling upon absorption, and no out-gassing during neutron irradiation.[15,19] DTO, for example, has previously been shown to have high chemical resistance for use as a neutron absorber in nuclear reactor control rods, having only a 1.7% increase in lattice volume under a neutron fluence of 3.5×10^{22} cm^{-2} and a comparable structural stability to the more

[a]Electronic addresses: simon.hall@bristol.ac.uk and Annela.Seddon@bristol.ac.uk

ubiquitous boron carbide.[15] The fact that DTO has not found widespread use though is because synthesis of the phase to a high enough purity is hampered due to the high stability of a competing Dy_2TiO_5 phase.[20]

1-monoolein (1-(*cis*-9-octadecenoyl)-*rac*-glycerol) is a highly versatile material that has aroused interest due to the range of mesophases it can form in water. It is widely used as an additive in the food industry and also has applications in both drug delivery and emulsion stabilization.[21–23] A type II amphiphile, monoolein becomes more curved with the addition of water, enabling stability in several complex, high curvature phases, such as the inverse bicontinuous cubic phases. However, the inclusion of additives into the monoolein/water system can lead to the formation of the L_3, or sponge phase, which is a disordered bicontinuous network of water tubules, separated by a lipid bilayer. It is a structured liquid phase, and contains larger pores than typically seen in the cubic phases, varying between 10 and 15 nm.[24] The water content of the pores can be altered using various additives, for example, 1,4-butanediol, polyethylene glycol (PEG) 400, t-butanol, and potassium thiocyanate.[23]

Here, we report a facile biomimetic sol-gel synthesis using the sponge phase formed by the lipid monoolein as a structure-directing template, resulting in high phase purity, mesoporous DTO, and GTO. The stability of monoolein in a 1,4-butanediol and water mixture complements the use of a simple sol-gel metal oxide synthesis route. By judicious control of the lipid/solvent concentration, the sponge phase of monoolein can be directly realised in the pyrochlore material, leading to a porous metal oxide network with an average pore diameter of 10 nm.

A complete description of the synthetic protocol can be found below, but briefly, a typical synthesis was as follows. Dysprosium and gadolinium nitrates were added to a mixture of water and 1,4-butanediol (volume ratio of 3:2), before the addition of monoolein and titanium butoxide. The addition of an alkoxide induced the formation of a gel, which was left to age prior to calcination in air leading to the final $Ln_2Ti_2O_7$ mesoporous products. Control samples were prepared via the same route but in the absence of monoolein.

Powder X-ray diffraction analysis of the pyrochlores synthesised via this lipid templated method showed that each target phase was formed to very high purity (Figure 1), displaying

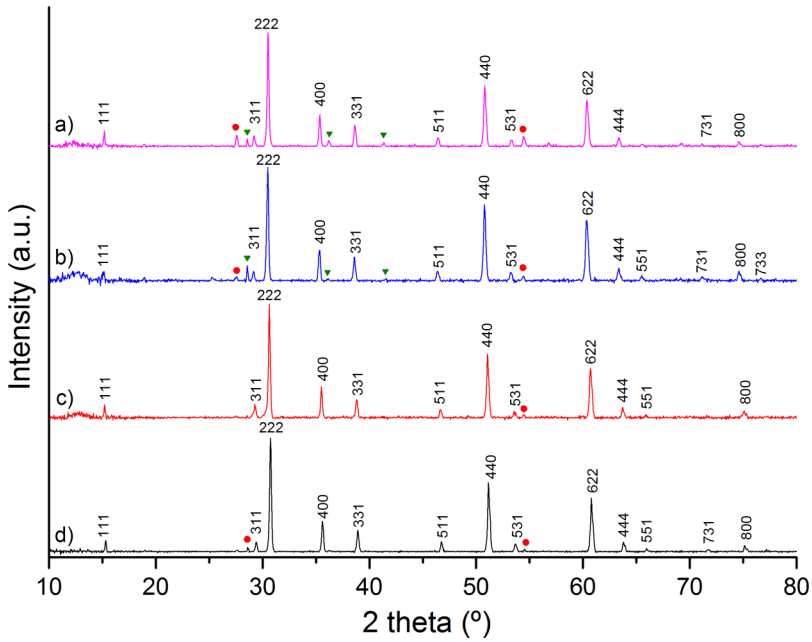

FIG. 1. Powder X-ray diffractograms of (a) templated $Gd_2Ti_2O_7$ JCPDS file no. 00-023-0259, (b) $Gd_2Ti_2O_7$ synthesised in the absence of template, (c) monoolein templated $Dy_2T_2O_7$ JCPDS file no. 00-017-0453, and (d) $Dy_2Ti_2O_7$ synthesised in the absence of template. Peaks labelled with circles and triangles represent TiO_2 (rutile phase, JCPDS file no. 01-073-1765) and Gd_2O_3 (JCPDS file no. 01-074-1987), respectively.

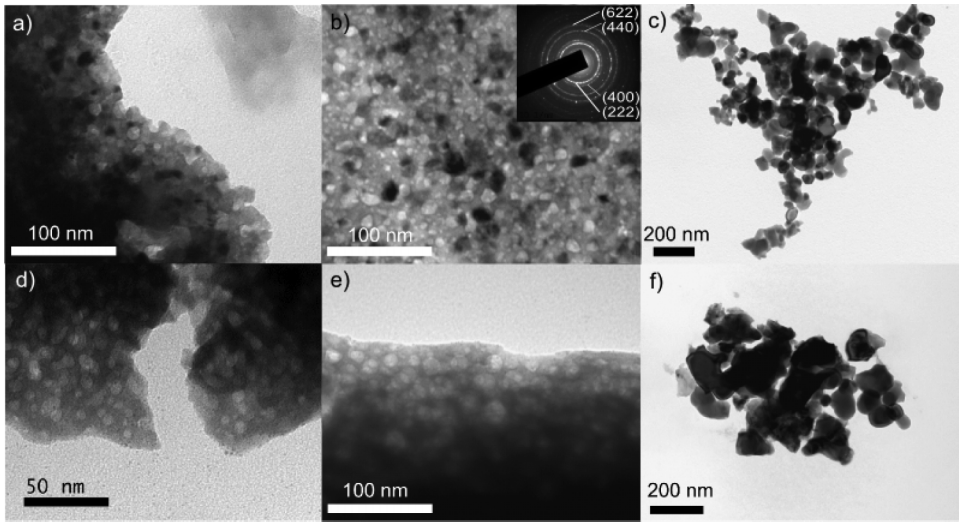

FIG. 2. Transmission electron micrographs of (a) and (b) $Dy_2Ti_2O_7$ synthesised in the presence of monoolein with an electron diffraction inset, (c) $Dy_2Ti_2O_7$ control, synthesised in the absence of template, (d) and (e) $Gd_2Ti_2O_7$ templated by monoolein, and (f) $Gd_2Ti_2O_7$ synthesised in the absence of template.

peaks consistent with a pyrochlore structure (JCPDS file no's. 00-017-0453 and 00-023-0259 for $Dy_2Ti_2O_7$ and $Gd_2Ti_2O_7$, respectively). Initial formation of the target phase was observed at 800 °C in both oxides (Figure S1 in the supplementary material).[25] A very small amount of aTiO_2 phase (rutile, JCPDS file no. 01-073-1765) was present in the final product.

The micromorphology of the samples was studied using Transmission and Scanning Electron Microscopy (TEM and SEM). Figures 2(a), 2(b), 2(d), and 2(e) show the mesoporous templated structures formed in the presence of monoolein. The monoolein-templated samples formed a mesoporous network, with pore sizes of 10 nm ± 4 nm and 12 nm ± 7 nm for DTO and GTO, respectively, which can be directly correlated to the 10 nm pores within the sponge phase of monoolein.[24,26,27] This result would suggest that the complex oxides are forming around the lipid bilayer and in effect being templated by the glycerol headgroups of monoolein. During the calcination process, both lipid and water will be removed from the structure, leaving behind a robust templated network. This is in distinct contrast to the sol-gel synthesis in the absence of monoolein (Figures 2(c) and 2(f)) which formed nanoparticulate $Ln_2Ti_2O_7$ crystals, with a measured crystallite size of 43 nm ± 15 nm and 25 nm ± 10 nm for DTO and GTO, respectively, correlating to the calculated values from Scherrer analysis of Figure 1 leading to values of 34 and 48 nm for DTO and GTO, respectively. It can be seen via SEM analysis (Figure 3) that the non-templated $Ln_2Ti_2O_7$ nanoparticles formed a porous network on aggregation with a pore size around 100 nm, an order of magnitude larger than the pores formed via monoolein templating. Energy-dispersive X-ray spectroscopy data for both sample sets can be seen in Figure S2 in the supplementary material.[25] Figure 4 shows the individual energy-dispersive X-ray analysis maps along with a layered image for the micrograph of each sample. Both samples show an even distribution of all elements in all of the $Ln_2Ti_2O_7$ samples.

Prior to calcination, small angle X-ray scattering (SAXS) (Figure 5) showed that the presence of metal nitrates within the lipid/water/1,4-butanediol mixture did not destroy the self-assembled monoolein bilayers within the L_3 structure, but increased the size of the unit cell with measured *d* spacings of 11.3 nm and 11.6 nm for the lipid alone and the lipid/metal salt solution, respectively. Due to the high X-ray absorption cross section of the calcined materials, it was not possible to obtain a SAXS pattern of the final products.

The specific surface area of the lanthanide titanates was measured by the Brunauer-Emmett-Teller (BET) method (Figure S3 in the supplementary material).[25] The measured specific surface areas of DTO templated and non-templated were 3.7 ± 0.2 and 7.8 ± 0.2 $m^2\ g^{-1}$, respectively, and of GTO, 3.9 ± 0.3 and 11.1 ± 0.2 $m^2\ g^{-1}$ for templated and non-templated samples, respectively.

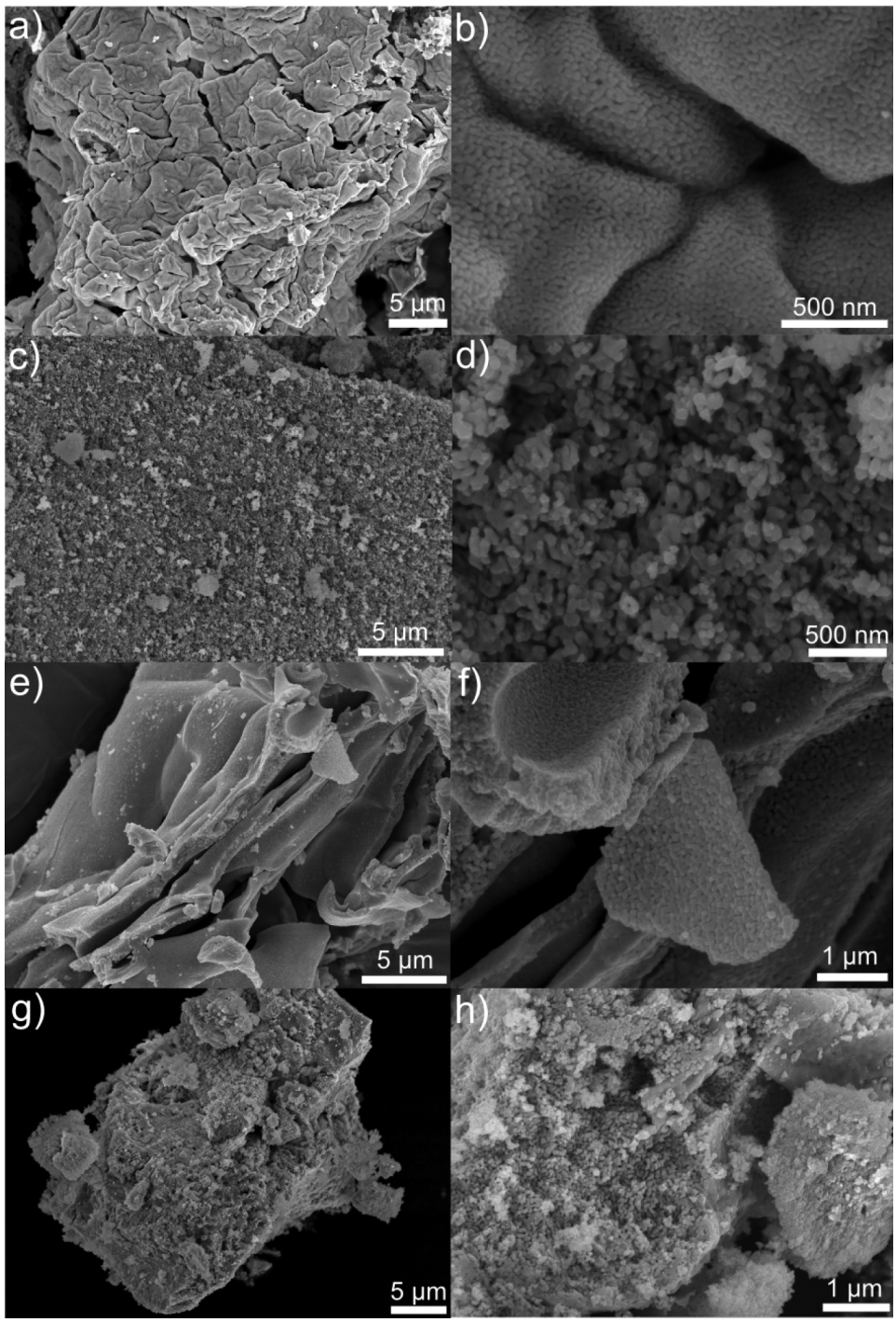

FIG. 3. SEM images of sample synthesised under various conditions. (a) and (b) monoolein templated $Dy_2Ti_2O_7$, (c) and (d) $Dy_2Ti_2O_7$ synthesised in the absence of a template. (e) and (f) $Gd_2Ti_2O_7$ monoolein templated oxides and (g) and (h) non-templated $Gd_2Ti_2O_7$.

The decrease of surface area in templated samples may be due to the lack of pore connectivity to the surface. It can be seen in Figure 2 that although there is a high number of surface pore openings, there are also many pores and tubules within the crystal that do not directly connect to the surface. High resolution SEM observations, Figures 3(b) and 3(f), confirm the lack of pores present at the surface of the material.

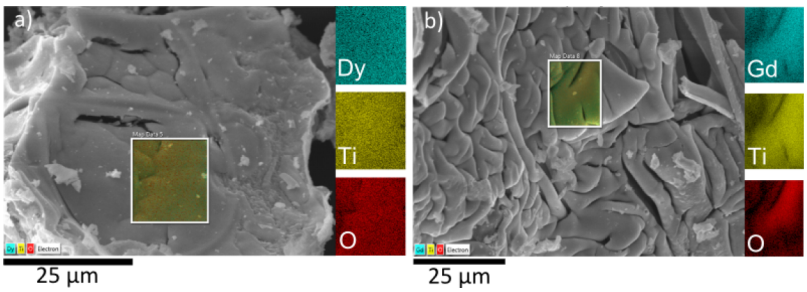

FIG. 4. SEM micrographs of (a) $Dy_2Ti_2O_7$ and (b) $Gd_2Ti_2O_7$ each with an inset of overlaid elemental mapping, the components of which can be seen on the right-hand side of each image. The measured X-rays were Dy Lα, Gd Lα, Ti Kα, and O Kα.

The neutron absorption of both non-templated and templated DTO materials determined at the ISIS pulsed neutron source (UK) is high in a wide neutron wavelength range from 0.1 to 4.5 Å, confirming their viability for use in neutron absorption applications (Figure 6), with the pyrochlore structure being maintained during irradiation (Figure S4 in the supplementary material).[25] The five dips in neutron transmission below 0.23 Å correspond to resonances of dysprosium isotopes.

In conclusion, we have demonstrated here a new route to high-purity mesoporous tertiary metal oxides based on a type II amphiphile sol-gel synthesis. When calcined, these gels produce highly pure mesoporous products, with pore sizes in close register to the 10 nm pores present in the lipid sponge phase system. This work is the first demonstration of a templated synthesis of any tertiary metal oxide using a type II amphiphile template and one that we believe represents a general and facile synthetic protocol for introducing controlled pore sizes in any metal oxide. With a high demand for controlled syntheses of complex functional materials with tailored morphologies, this report represents an important advance in their synthesis.

Materials: Dysprosium nitrate hydrate, gadolinium nitrate hexahydrate, titanium butoxide, and 1,4-butanediol were all purchased from Sigma-Aldrich UK and were used as received. Monoolein in the form of Rylo was kindly donated for research by Danisco.

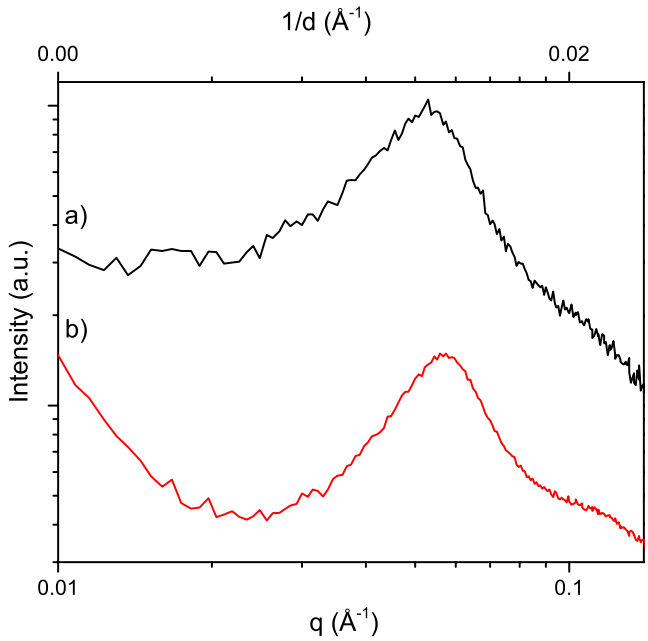

FIG. 5. 1D SAXS pattern for (a) monoolein/water/1,4-butanediol system in presence of $Dy(NO_3)_3$ and (b) monoolein/water/1,4-butanediol system.

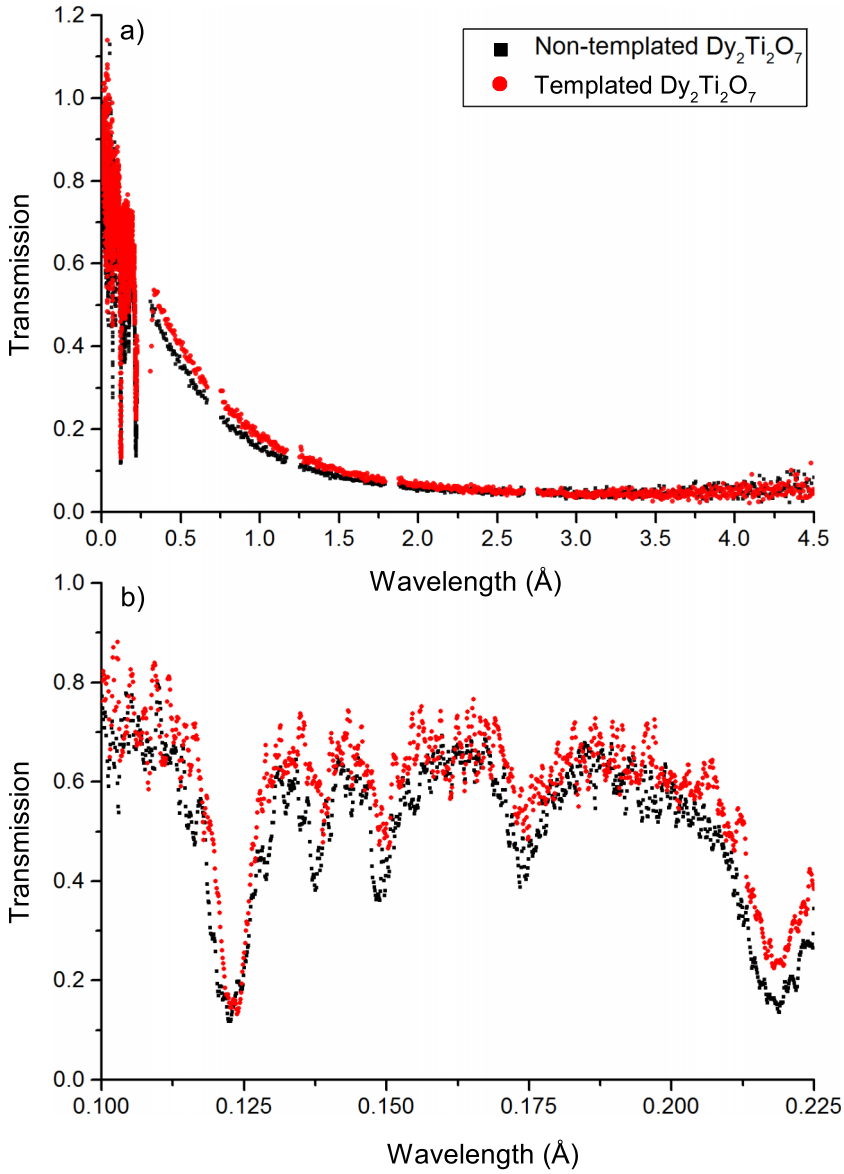

FIG. 6. (a) Neutron transmission curves of 10 mm thick non-templated $Dy_2Ti_2O_7$ and monoolein templated $Dy_2Ti_2O_7$; (b) expanded high-energy region of the transmission spectra exhibiting Dy resonances.

Lipid sol-gel synthesis: Dysprosium nitrate hydrate, or gadolinium nitrate hexahydrate (1.5 g and 1.94 g, respectively) was dissolved in deionised water (3 ml) and then mixed with 1,4-butanediol (2 ml), stirred until the formation of a homogenous mixture. Monoolien (3.3 g) was slowly integrated with the mixture, followed by the addition of titanium butoxide (1.5 g) where gelation commenced immediately. The mixture was allowed to age for a week before calcination in air at 900 °C at a ramp rate of 3 °C min^{-1}. Control samples were synthesised via the same route, in the absence of monoolein.

Characterization of materials: Powder X-Ray Diffraction (XRD) analyses were performed, using a Bruker (Billerica, USA) D8 Advance Powder X-ray Diffractometer (Cu K_α radiation, $\lambda = 1.54$ Å) at 2θ values of 20°–80°, with a step size of 0.05° at a step rate of 2.25 s. JEOL JEM 1200 EX and JEOL 1400 transmission electron microscopes were used along with JEOL field emission gun 6330 and IT300 scanning electron microscopes to observe the morphology of the oxides synthesised. An Oxford Instruments energy-dispersive X-ray instrument was used in

conjunction with SEM to confirm the presence of all elemental species within the material. SAXS measurements were performed using a GANESHA 300 XL (SAXSLAB, Copenhagen, Denmark) SAXS system with an adjustable sample to detector distance set to 1.041 m. X-rays were detected using an in-vacuum Pilatus 300k (Dectris, Baden, Switzerland) detector and were generated using a sealed tube generator with a Cu anode (X-ray wavelength 1.54 Å). Fluid samples were loaded into reuseable 1.5 mm quartz-glass capillary cells. For a typical experiment, measurements were performed for 10 min. A transmission-normalised solvent background was subtracted from the data, and sections of the image not caused by X-ray scattering, such as the beamstop, were masked out of the image. The data were then radially averaged to produce one-dimensional scattering curves for further analysis. BET measurements were taken on a Micromeritics 3-Flex gas sorption analyser. All samples were degassed at 150 °C for 6 h under dynamic vacuum prior to analysis adsorption measurements and were run using nitrogen at 77 K. Neutron transmission measurements were undertaken on the ROTAX beamline at the ISIS facility using the time-of-flight technique. The samples of 10 mm thickness were exposed at 15.85 m from the pulsed source to a wide range of incident neutron wavelengths, from 0.1 to 4.5 Å (energies: 4 meV–8 eV), mounted in front of a neutron imaging camera based on microchannel plates.

S.R.H. and N.B. would like to acknowledge Sasol Technology UK Ltd. and the Engineering and Physical Sciences Research Council (EPSRC), UK (Grant No. EP/G036780/1), and the Bristol Centre for Functional Nanomaterials for project funding. S.R.H. and N.B. would like to thank Professor James Annett and Dr. Daniel Fritsch of the School of Physics, University of Bristol. The authors would like to thank A. Tremsin of UC Berkeley for the use of a microchannel plate detector during neutron imaging tests. The Ganesha X-ray scattering apparatus and electron microscopy carried out by the Chemical Imaging Facility, University of Bristol in this research were funded under the EPSRC Grant "Atoms to Applications," Grant No. EP/K035746/1.

[1] B. Vaidhyanathan, P. Raizada, and K. J. Rao, J. Mater. Sci. Lett. **16**, 2022 (1997).
[2] A. F. Fuentes, K. Boulahya, M. Maczka, J. Hanuza, and U. Amador, Solid State Sci. **7**, 343 (2005).
[3] Z. Shen, Y. Li, Q. Hu, W. Luo, and Z. Wang, "Dielectric properties of B–site charge balanced Dy–doped $SrTiO_3$ ceramics for energy storage," J. Electroceram. (in press).
[4] B. Xiang, P. Wang, X. Zhang, S. A. Dayeh, D. P. R. Aplin, C. Soci, D. Yu, and D. Wang, Nano Lett. **7**, 323 (2007).
[5] R. C. Smith, T. Ma, N. Hoilien, L. Y. Tsung, M. J. Bevan, L. Colombo, J. Roberts, S. A. Campbell, and W. L. Gladfelter, Adv. Mater. Opt. Electon. **10**, 105 (2000).
[6] T. Maruyama and K. Fukui, Thin Solid Films **203**, 297 (1991).
[7] M. Niederberger, Acc. Chem. Res. **40**, 793 (2007).
[8] R. Sui and P. Charpentier, Chem. Rev. **112**, 3057 (2012).
[9] W. Li, A. Lu, C. Weidenthaler, and F. Schüth, Chem. Mater. **16**, 5676 (2004).
[10] Y. Sakamoto, A. Fukuoka, T. Higuchi, N. Shimomura, S. Inagaki, and M. Ichikawa, J. Phys. Chem. B **108**, 853 (2004).
[11] D. Gu and F. Schüth, Chem. Soc. Rev. **43**, 313 (2014).
[12] S. Akbar, J. M. Elliott, M. Rittman, and A. M. Squires, Adv. Mater. **25**, 1160 (2013).
[13] N. Cruise, K. Jansson, and K. Holmberg, J. Colloid Interface Sci. **241**, 527 (2001).
[14] K. Holmberg, J. Colloid Interface Sci. **274**, 355 (2004).
[15] V. D. Risovany, E. E. Varlashova, and D. N. Suslov, J. Nucl. Mater. **281**, 84 (2000).
[16] T. Fennell, O. A. Petrenko, G. Balakrishnan, S. T. Bramwell, J. D. M. Champion, B. Fåk, M. J. Harris, and D. McK. Paul, Appl. Phys. A: Mater. Sci. Process. **74**, 889 (2002).
[17] L. D. C. Jaubert and P. C. W. Holdsworth, J. Phys.: Condens. Matter **23**, 164222 (2011).
[18] S. Saha, D. V. S. Muthu, C. Pascanut, N. Dragoe, R. Suryanarayanan, G. Dhalenne, A. Revcolevschi, S. Karmakar, S. M. Sharma, and A. K. Sood, Phys. Rev. B **74**, 064109 (2006).
[19] L. G. Shcherbakova, L. G. Mamsurova, and G. E. Sukhanova, Russ. Chem. Rev. **48**, 228 (1979).
[20] A. Sinha and B. P. Sharma, J. Am. Ceram. Soc. **88**, 1064 (2005).
[21] A. Ganem-Quintanar, D. Quintanar-Guerrero, and P. Buri, Drug Dev. Ind. Pharm. **26**, 809 (2000).
[22] R. F. Turchiello, F. C. B. Vena, Ph. Maillard, C. S. Souza, M. V. B. L. Bentley, and A. C. Tedesco, J. Photochem. Photobiol., B **70**, 1 (2003).
[23] C. V. Kulkarni, W. Wachter, G. Iglesias-Salto, S. Engelskirchen, and S. Ahualli, Phys. Chem. Chem. Phys. **13**, 3004 (2011).
[24] A. Ridell, K. Ekelund, H. Evertsson, and S. Engström, Colloids Surf., A **228**, 17 (2003).
[25] See supplementary material at http://dx.doi.org/10.1063/1.4930808 for this figure.
[26] V. Cherezov, J. Clogston, M. Z. Papiz, and M. Caffrey, J. Mol. Biol. **357**, 1605 (2006).
[27] A. M. Seddon, G. Lotze, T. S. Plivelic, and A. M. Squires, J. Am. Chem. Soc. **133**, 13860 (2011).